OPTICAL NONLINEARITIES IN PLASMONIC NANOSUSPENSIONS

A thesis presented to the faculty of
San Francisco State University
In partial fulfillment of
The Requirements for
Physics

Master of Science
In
Physics

by

Trevor S. Kelly

San Francisco, California

August 2017

CERTIFICATION OF APPROVAL

I certify that I have read *OPTICAL NONLINEARITIES IN PLASMONIC NANOSUSPENSIONS* by Trevor S. Kelly and that in my opinion this work meets the criteria for approving a thesis submitted in partial fulfillment of the requirements for the degree: Master of Science in Physics at San Francisco State University.

Zhigang Chen
Professor of Physics

Roger Bland
Professor Emeritus of Physics

Huizhong Xu
Associate Professor of Physics

OPTICAL NONLINEARITIES IN PLASMONIC NANOSUSPENSIONS

Trevor S. Kelly
San Francisco State University
2017

Optical nonlinearities in colloidal nanosuspensions are due to a nonlinear change in the refractive index, brought about by the interaction of light and nanoparticles. In this work we explore these light particle interactions, and present theory and experimental verification of our claims. First we demonstrate coupled beam propagation dynamics in colloidal gold nanosuspensions. We achieve guidance of an infrared (IR) probe beam (1064 nm) by a low-power visible beam (532 nm) in a gold nanosphere and nanorod suspensions, due to the formation of a plasmonic resonant soliton. We also show soliton-mediated orientational ordering of gold nanorods in a gold nanorod suspension. The orientation of the nanorods along the waveguide is regulated by the optical torque exerted by the linearly polarized soliton beam. We observe orientation-enhanced birefringence along the soliton channel by measuring the polarization transmission spectrum of a probe beam (1064 nm), suggesting a disorder-to-order transition of nanorods due to the action of the soliton beam.

I certify that the Abstract is a correct representation of the content of this thesis.

Chair, Thesis Committee Date

ACKNOWLEDGMENTS

I would like thank Dr. Zhigang Chen for giving me the opportunity to work and learn in his lab, and for his support and assistance on all of the projects I have worked on during my time at San Francisco State University, which has been an amazing experience. I would like to thank my committee members, Dr. Roger Bland, Dr. Weining Man and Dr. Huizhong Xu. Dr. Bland was an integral part of my admission into the program and assisted me with my experimental and computational questions. Dr. Weining Man was an immense help with my understanding of real world of physics and it's applications. Dr. Xu was essential for taking our research to a new level, and I appreciate the time and work he contributed. I would like to thank the postdoctoral fellows that I have had the pleasure to learn from and work with. Dr. Yuxuan-Ren was with me through the countless hours of experimental and theoretical work, we accomplished a great deal together. Dr. Akbar Samadi taught me my very first lessons in experimental optics, and I owe him for my experimental skills. Dr. Anna Bezryadina encouraged me to join the lab, and got me started down this path and helped me the whole way. Dr. Young Son and Dr. Rekha Gautam also assisted in our research. I would also like to thank all the students I have had the pleasure of working with in the lab, Dan Gallardo, Drew Bischel, Chensong Zhang, Graham Siggins, Steven Nenni, Jeff Butler, Josh Lamstein and PJ Alvero. They were

essential for our Optical Society activities. I would also like to thank all the professors in the Physics and Astronomy Department at San Francisco State University, for their hand in my physics education. I would also like to thank all the collaborators that we have worked with on our various projects. Finally I would like to thank Dr. Barbara Neuhauser, for starting me in physics research.

Contents

List of Figures

Chapter 1

Introduction

The unique optical properties of artificial soft-matter systems have been the subject of extensive research since Ashkin's early pioneering work, where the use of liquid suspensions of submicrometer particles was shown to mimic artificial Kerr like media [1]. For example, colloidal suspensions containing dielectric micro- or nanoparticles have been shown to exhibit nontrivial nonlinearities that could lead to modulation instability and optical spatial solitons [2, 3, 4, 5, 6, 7, 8, 9, 10, 11, 12]. These nonlinearities can be understood to be a consequence of optical force-induced refractive index changes. In colloidal suspensions, the micro- or nanoparticles will be either attracted or repelled by a laser beam, depending on whether the sign of their optical polarizability is positive or negative, respectively [5, 10]. Typically, suspended particles have a positive polarizability (PP), since they have a higher refractive index than the background solution, thus promoting enhanced scattering and a catastrophic beam collapse [5, 8]. Recently, however, deep penetration of

light through scattering dielectric nanosuspensions has been achieved through different mechanisms [9, 10, 11, 12]. Furthermore, robust propagation of self-trapped light over distances exceeding 25 diffraction lengths has been demonstrated in plasmonic nanosuspensions [13]. Guiding and steering light has also been observed in colloidal suspensions of dielectric(polystyrene), as well as metallic (silver) nanoparticles [14, 15]. This work will focus on the coupled beam dynamics of guiding and steering of light in nanoparticle suspensions, how this can be used to manipulate particle motion and in particular nanorod orientation, and how we can demonstrate these effects by experimental methods.

Chapter 2

Guiding and nonlinear coupling of light in plasmonic nanosuspensions

In this chapter we will explain how a soliton channel is formed and how this can lead to guidance of another beam at a wavelength far off resonance[16]. We will be dealing mainly with coupled beam propagation dynamics in colloidal gold nanosuspensions. In this chapter, we guide an infrared (IR) probe beam (1064 nm) by a low-power visible beam (532 nm) in a gold nanosphere or in nanorod suspensions due to the formation of a plasmonic resonant soliton. Although the IR beam does not experience nonlinear self-action effects, even at high power levels, needle-like deep penetration of both beams through otherwise highly dissipative suspensions is realized.

2.1 Self-induced waveguides

First let us discuss self-induced waveguides, and the fact that they can be established in colloidal nanosuspensions through the formation of plasmonic resonant solitons. The soliton-induced waveguides are typically 4 cm long and, in principle, can exceed those observed in organic glasses or nonlinear crystals [17, 18]. The wavelength-dependent optical nonlinearity in a plasmonic nanosuspension can be exploited in such a way so that linear guidance of a strong infrared (IR) optical beam (as a "probe") can be achieved through a weak visible soliton-forming beam (used as a "pump"). The guided IR output pattern depends on the input power of the self-trapping beam. In later chapters we will discuss the master/slave-type nonlinear coupling and how it is observed in gold nanoshell suspensions, in which both the probe and pump beams contribute to the self-focusing nonlinearity.

2.1.1 Self-induced waveguides setup

To physically achieve our desired results, we use an optical experimental set up, which is illustrated in Fig. 2.1, where a continuous-wave (CW) laser operating at $\lambda = 532$ nm (green) is used as the pump, while another CW laser operating at an IR wavelength ($\lambda = 1064$ nm) is used as the probe. Both beams propagate collinearly through a 4 cm long cuvette containing different nanoparticle (gold nanosphere, nanorod, or nanoshell) suspensions. The green beam passes through a half-wave plate and polarizing beam splitter (not shown in Fig. 2.1) so that its power can be

adjusted, and it is expanded/collimated before being focused near the input facet of the sample.

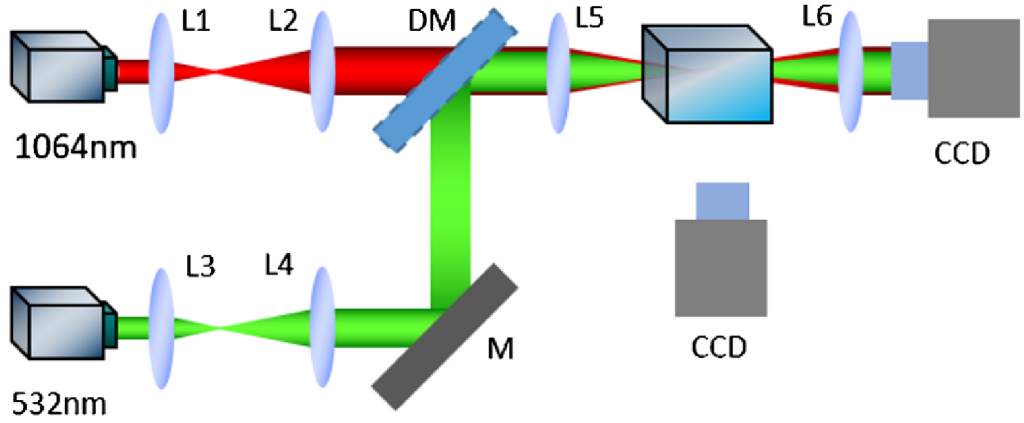

Figure 2.1: Schematic of the experimental setup.

Fig. 2.1. Schematic of the experimental setup. An IR beam (as a probe) is combined with a green beam (as a pump), propagating collinearly through a sample (a 4 cm cuvette containing a nanosuspension). The images of input/output transverse intensity patterns and the side view of the beam propagation are taken by CCDs.

The IR beam is also expanded/collimated and is combined with the green beam through a dichroic mirror before being focused together by a lens with a focal length of 80 mm. The diameters of the collimated green and IR beams are 5.0 and 6.5 cm, respectively, and the corresponding beam sizes at the focal plane are measured to be 21.4 and 16.6 μm. The beam propagation through the sample is monitored with different cameras. The side views of the visible light beam are taken with a regular

Canon camera, while those of the IR beam are taken using a CCD camera (Thorlabs, USB 2.0), together with a Zeiss microscope eyepiece for magnification. Another CCD camera (Coherent, USB 2.0) assisted with a BeamView imaging system is used to record the input/output beam profiles before and after the cuvette. Due to the long sample and the two wavelengths used, the imaging system is slightly adjusted for each experiment to ensure that the camera can image the desired locations through the sample for both wavelengths.

2.1.2 Guiding an IR beam by a green soliton beam

The green pump beam can create self-trapped channels in nanoparticle suspensions through the formation of plasmonic resonant solitons [13]. Specifically, the optical gradient force on a suspended particle is not only intensity dependent, but is also dependent on the polarizability of a particular nanosuspension. The sign of the polarizability is determined by the relative index of refraction between the particles and the background medium. Particles with PP in the suspension are pulled into the path of the laser beam, whereas particles with negative polarizability (NP) in the suspension are repelled by the beam. In either case, the light-particle interaction leads to a nonlinear optical response because of an increase in the refractive index along the beam path that leads to self-focusing. This self-focusing nonlinearity allows a beam to penetrate a long colloidal suspension of nanoparticles that would have been otherwise impossible because of diffraction, diffusion, and scattering [10,

13]. We will now focus on linear guiding and nonlinear coupling of optical beams in such nanosuspensions.

The first guiding experiment is conducted in an aqueous suspension containing gold nanospheres with an average diameter of 40 nm [Fig. 2.2(a)].

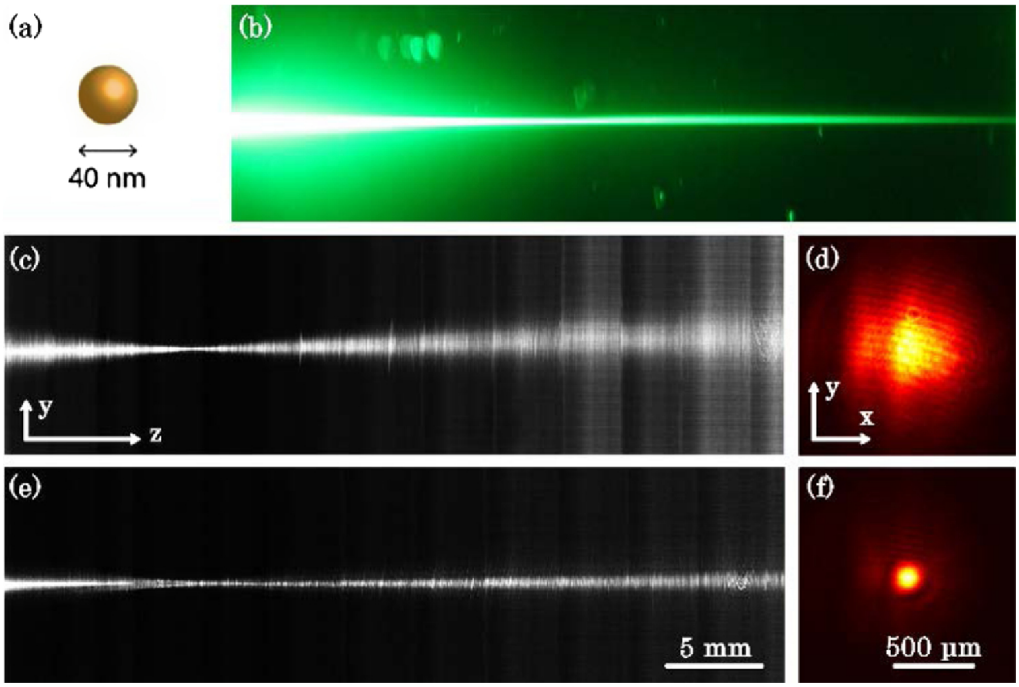

Figure 2.2: Guiding an IR beam by a green soliton beam in a colloidal suspension of gold nanospheres.

Fig. 2.2. Guiding an IR beam by a green soliton beam in a colloidal suspension of gold nanospheres. (a) Illustration of a gold nanosphere. (b) Side view of the soliton beam. (c), (d) Side view and transverse output pattern of the IR probe beam in the linear diffraction regime when the soliton beam is absent. (e), (f) Corresponding

results when the soliton beam is present. (The IR side-view pictures were composed of hundreds of superimposed images due to weak scattering at the IR wavelength.)

The "pump" or soliton-forming beam is focused inside, but near the front facet of the cuvette. As the power for the green beam is increased gradually, a self-trapped channel is formed at an output power of only 60 mW, as seen by the side view of the soliton beam [Fig. 2.2(b)]. According to theoretical calculations [13], the gold nanospheres in the suspension are positively polarized at 532 nm, experiencing low scattering, but strong, absorption at this wavelength. Particles are attracted along the beam path, which leads to self-trapping of the beam without a beam collapse at lower power levels. This is attributed to a combined action of optical force-induced self-focusing nonlinearity and self-defocusing thermal effects, which gives rise to a cubic-quintic nonlinear response in the colloidal suspension [13, 15].

When an IR probe beam is launched into the same nanosphere suspension (without the green soliton beam), it does not experience appreciable nonlinear self-action, even when its power is increased to 500 mW. Instead, the IR beam tends to diffract in the suspension, as shown from the side view. [Fig. 2.2(c)] and the cross-sectional output [Fig. 2.2(d)]. However, once the green soliton beam is switched on, the IR beam is guided and is well confined in the soliton-induced waveguide [Figs. 2.2(e) and 2.2(f)]. For the results obtained in Fig. 2.2, the power of the probe beam is about 50 mW. Linear diffraction of an IR probe beam (with the soliton beam off) and guidance (with the soliton beam on) is observed for a wide range (20–500 mW)

of input power, although more pronounced guidance is realized at a low power as opposed to a high power. It should be pointed out that the 1064 nm wavelength is far away from the plasmonic resonance of the gold nanosphere and, hence, is subjected to very weak absorption and scattering [13]. In fact, since our camera is not very sensitive to IR light and the scattering from the IR beam is so weak, we had to develop a scheme (by combining integration and scanning) to construct the side-view images shown in Figs. 2.2(c) and 2.2(e). This was achieved by taking a short movie at different sections across the sample length and then superimposing all image frames (up to 2000 frames for a movie of 4 min) taken from the scattered light for each section to reconstruct the side view of the probe beam across the entire sample. I would like to thank Dr. Roger Bland for his help on the coding to superimpose the images.

We then performed similar experiments in a colloidal suspension of gold nanorods. The gold nanorods employed for our experiment have an average diameter of 50 nm and a length of 100 nm [Fig. 2.3(a)].

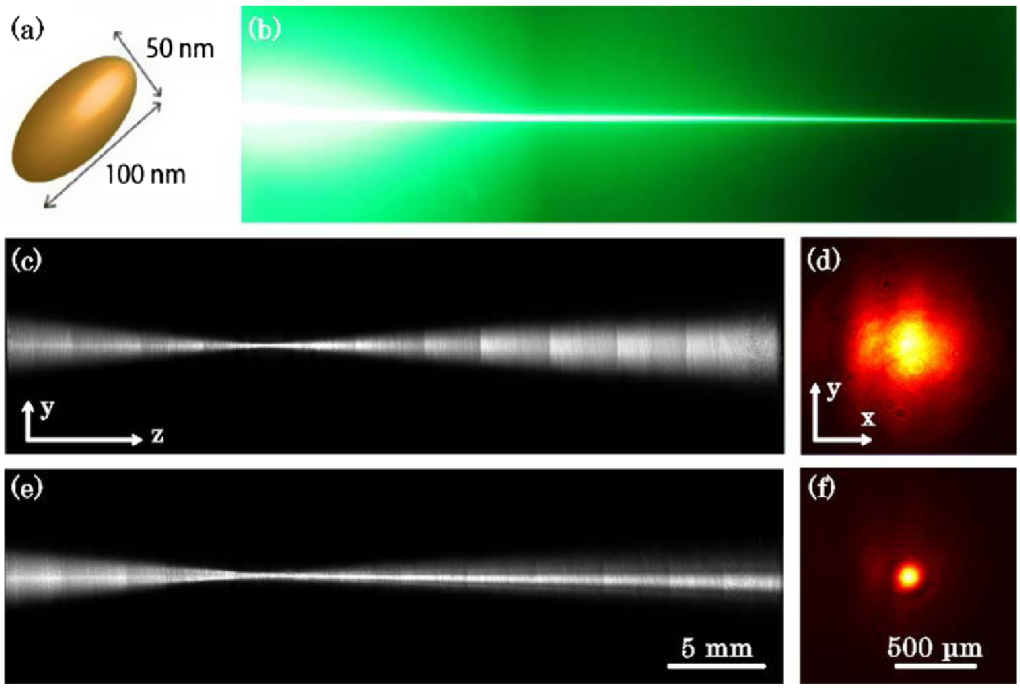

Figure 2.3: Guiding an IR probe beam by a green soliton beam in a colloidal suspension of gold nanorods.

Fig. 2.3. Guiding an IR probe beam by a green soliton beam in a colloidal suspension of gold nanorods. (a) Illustration of a gold nanorod. (b) Side view of the soliton beam. (c), (d) Side view and transverse output pattern of the IR probe beam in the linear diffraction regime when the soliton beam is absent. (e), (f) Corresponding results when the soliton beam is present. (The IR side-view pictures were composed of hundreds of superimposed images due to weak scattering at the IR wavelength.)

Analysis suggests that [13] the polarizability for an aqueous suspension of such

gold nanorods is negative at 532 nm. Nevertheless, since the particles are effectively pushed away from the beam center, nonlinear self-focusing still occurs [10, 13]. Figure 2.3(b) shows a typical experimental result of a self-trapped channel of the green beam observed at a power of 100 mW. On the other hand, the IR beam alone again to ∼1 W. As shown in Figs. 2.3(c) and 2.3(d), the IR beam itself displays no nonlinear self-action at a power of 50 mW. However, when the green soliton beam is turned on, the guidance of the IR beam into the soliton-induced waveguide channel is reestablished [Figs. 2.3(e) and 2.3(f)].

We can see, that even though the colloidal gold nanospheres and nanorods have different polarizability signs at 532 nm, linear guidance of the IR beam can be observed in both suspensions. This confirms that, in both PP and NP suspensions, optical force-induced nonlinearity can elevate the refractive index, thus establishing a waveguide along the beam path, which guides not only the soliton beam, but also another beam at a wavelength far off plasmonic resonance.

2.1.3 Introduction of weak nonlinearity by pump beam

Although the IR beam by itself is not capable of forming a self-trapped channel, and its confinement in these nanosuspensions is mainly due to the guidance provided by the green soliton-induced waveguide, the presence of the IR probe beam slightly changes the output patterns of both beams. This can be seen from the guided output pattern of the probe beam that directly depends on the input power of the

self-trapped green beam. As seen in Fig. 2.4, after the green beam is self-trapped (at 60 mW for the gold nanosphere [Fig. 2.4(a)] and 100 mW for nanorod suspensions [Fig. 2.4(d)]), it becomes more focused when the probe is sent through, although some intensity is lost to a concentric ring around the guided beam. If the the soliton beam power is reduced, the concentric ring fades away and the focused beam is restored, but with a loss of sharpness.

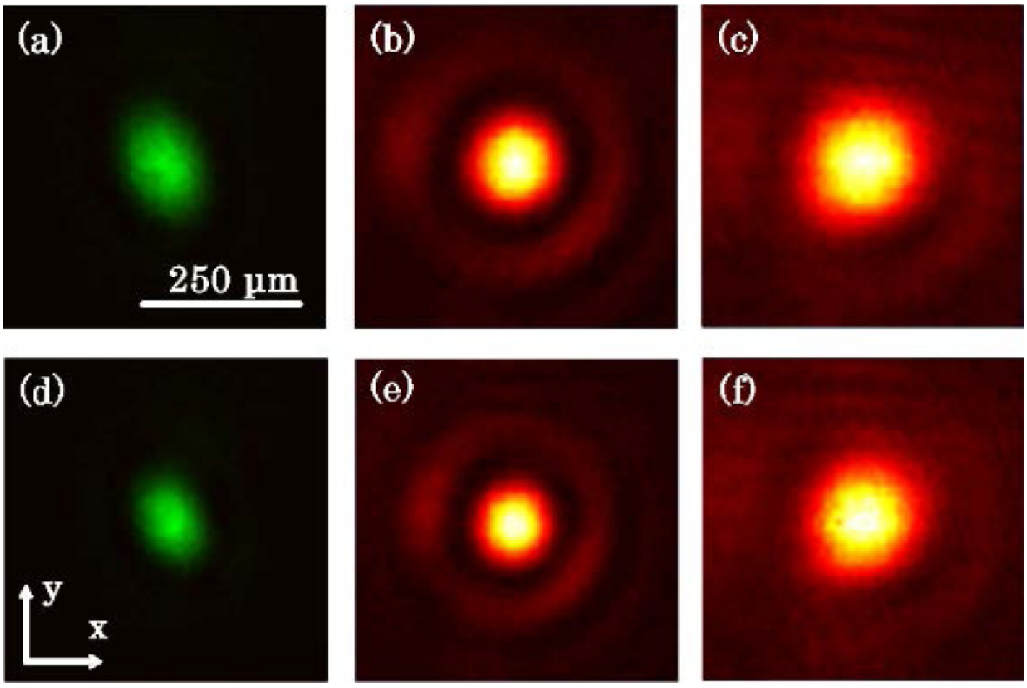

Figure 2.4: Transverse output patterns of the self-trapped green pump beam and the guided IR probe beam at different pump beam powers.

Fig. 2.4. Transverse output patterns of the (a), (d) self-trapped green pump beam and (b), (c), (e), (f) the guided IR probe beam at different pump beam powers. (a)–(c) For gold nanospheres when the green beam power is decreased from (b) 60 to (c) 30 mW. (d)–(f) For gold nanorods when the green beam power is decreased from (e) 100 to (f) 40 mW. The power of the probe beam is kept at 50 mW.

The change in the guided output patterns of the probe beam due to a reduction of the soliton beam power is shown in the second and third columns of Fig. 2.4. Our

results indicate that, after introducing the probe beam, the power of the pump beam needs to be reduced to maintain a Gaussian profile output, with a clean self-trapped channel. While the dynamics of this beam interaction need to be explored further, this suggests that the IR beam, although far away from the plasmonic resonance, could introduce a weak nonlinearity.

Chapter 3

Vector-type nonlinear coupling

Now we deal with coupled beam propagation dynamics in a colloidal gold nanoshell suspension, in which the nanoparticles have opposite polarizabilities at the visible and IR wavelengths where both beams experience a self-focusing nonlinearity that can be fine-tuned. Using this interaction we demonstrate a master/slave vector-type nonlinear coupling between the green and IR beams mentioned in the previous chapter. The nonlinear coupling is accomplished in silica-gold core-shell nanosuspensions, since both the green and IR beams can exhibit appreciable nonlinearities. The nanoshell particles have an average silica-core radius of 60 nm and a gold-shell thickness of 15 nm [Fig. 3.1(a)]. The nanoshells in an aqueous suspension exhibit an NP at 532 nm, but a PP at 1064 nm, as seen from the light blue curve in the theoretical calculation [13] shown in Fig. 3.1(b). In such a soft-matter environment, we observe a tunable nonlinear coupling between the two beams by varying the relative strength of nonlinearities due to the competing PP and NP effects exhibited

at 1064 and 532 nm, respectively. At appropriate low intensities, both beams are unable to create self-trapped channels alone; yet, they achieve mutual self-trapping when both are present (coupled). At the coupled regime with one beam dominant, the dominant beam exhibits a nonlinearity higher than that of the pairing beam, resulting in the self-focusing abilities being less affected after removal of the pairing beam (decoupled). Typical experimental results are shown in Fig. 3.1.

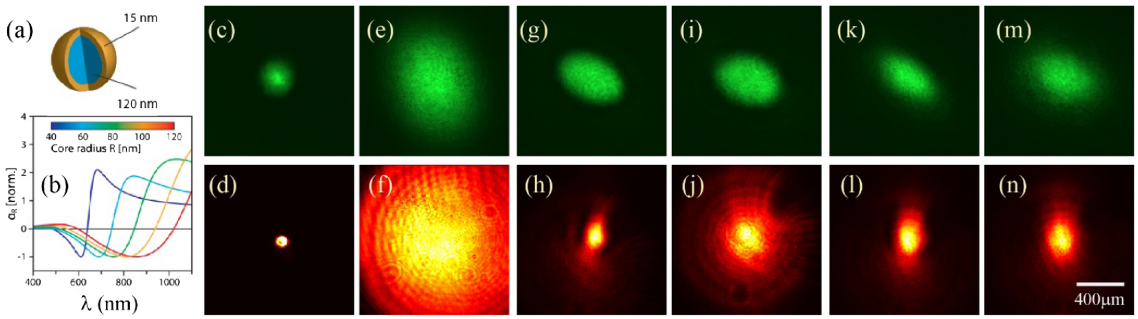

Figure 3.1: Nonlinear coupling of a green beam and an IR beam in the colloidal suspensions of gold nanoshells.

Fig. 3.1. Nonlinear coupling of a green beam (top) and an IR beam (bottom) in the colloidal suspensions of gold nanoshells. (a) Illustration of a core-shell nanoparticle with a silica-core diameter of 120 nm and a gold-shell thickness of 15 nm. (b) Plot of calculated polarizability vs. wavelength for different particle sizes. [13] (c), (d) Transverse intensity patterns of focused input beams. (e), (f) Linear diffraction output after 4 cm of propagation through the nanosuspension. (g), (h) Nonlinear coupled output when the green beam has a dominant nonlinearity, so the green beam remains self-trapped, but the IR beam exhibits only partial focusing after being decoupled, i.e., when the other coupling beam is removed (i), (j). (k)–(n) Similar to (g)–(j), except that the IR beam has a dominant nonlinearity.

The coupling and decoupling scheme is similar to that used for an earlier demonstration of a coupled soliton pair or vector soliton [19]. Figures 3.1(c)–3.1(f) show the beam patterns near the focal point and their linear diffraction after 4 cm of propagation through the suspension. Figures 3.1(g)–3.1(j) show this nonlinear coupling

when both the green and IR beams are present and undergo nonlinear self-focusing, but the green beam dominates (i.e., exhibits a higher nonlinearity). This can be seen since the green beam is affected less after removing its partner beam (decoupled). Likewise, when the IR beam dominates [Figs. 3.1(k)–3.1(n)], the green beam experiences less self-focusing when it is decoupled from the IR beam, whereas the IR beam does not show significant change when the green beam is blocked. It should be pointed out that a perfect balance of the nonlinear action between the two beams is difficult to reach in an experiment with the current selection of wavelengths. However, it is possible that using the green beam, λ= 532 nm along with a red beam, λ= 800 nm should produce better results.

Chapter 4

Soliton-mediated orientational ordering of gold nanorods and birefringence in plasmonic suspensions

As was shown in previous chapters, the soliton can have particles inside or outside the channel, depending on the sign of polarizability. This raises the question, is the soliton beam able to induce ordering of the nanorods? In the upcoming sections we show [20] that this is a possible and measurable phenomenon. This soliton-induced ordering also leads to birefringence/dichroism in the nanorod plasmonic suspension.

4.1 Soliton-mediated orientational ordering

In this chapter we will deal with soliton-mediated orientational ordering of gold nanorods in a colloidal plasmonic suspension . Due to the nonlinear optical response of the suspension, a light beam forms an optical spatial soliton which creates an effective optical waveguide. The orientation of the nanorods along the waveguide is regulated by the optical torque exerted by the linearly polarized soliton beam. By measuring the polarization transmission spectrum of a probe beam at a wavelength far from the plasmonic resonance, we observe orientation-enhanced birefringence along the soliton channel, suggesting a disorder-to-order transition of nanorods due to the action of the soliton beam. This approach may be applied in other colloidal systems with optical force-induced nonlinearity.

4.1.1 Two different types of coupled beam propagation dynamics

Metallic nanoparticles have widespread applications due to the tunability of their optical, plasmonic, and photothermal properties [21, 22, 23]. The plasmonic resonance of the nanorods can be controlled by tuning their size and shape, resulting in different responses to light frequency, polarization, and momentum [22, 13]. In optical trapping experiments, it has been demonstrated that an optical beam with angular momentum can rotate either birefringent or absorbing particles [24, 25, 26], and that an optical wrench produced by circularly polarized light can allow for the detection of the torque on a DNA tethered to the birefringent particle [25]. Even

a linearly polarized beam is sufficient to optically align anisotropic particles due to the anisotropic polarizability [24]. In particular, both the optical trapping and the fluorescence correlation spectroscopy experiments have revealed that a single plasmonic nanorod trapped with a near-infrared (IR) laser tends to reconfigure itself to orient with the light polarization [27, 28, 29], apart from other experiments such as polarization-dependent white-light transmission spectrum [30]. A theoretical study with the Maxwell tensors also revealed that elongated gold nanorods tend to align themselves with the long axis parallel to the beam polarization when the wavelength of light is greater than that of the longitudinal surface plasmon resonance (LSPR) [31]], but perpendicular to the polarization when the wavelength is smaller than that of the LSPR [31, 32, 33]. This orientation effect, originating from the optically induced torque, could bring about phase change and optical anisotropy for the nanorod ensembles [28, 30, 34, 35].

4.1.2 Previous studies

Our previous studies have demonstrated that even an off-resonant laser beam could create a soliton channel in gold nanorod suspensions, thanks to the strong self-focusing nonlinearity originated from optical forces [13, 16]. In the following sections, we demonstrate optical soliton-induced orientational ordering of nanorods in the gold nanoparticle suspensions. By sending a probe beam with varying linear polarization into the soliton channel, we measure the polarization transmission

spectrum and compare with the cases when there is no soliton beam, or the soliton beam is circularly polarized. The polarization-dependent modulation in transmitted power, observed only when the soliton beam is linearly polarized, is attributed to birefringent absorption (difference in the imaginary part of the refractive index) as a result of soliton-induced reorientation of gold nanorods). Similar experiments with gold nanosphere suspensions led to soliton formation, but not the enhanced birefringence. The observed phenomenon is fundamentally different from those due to optically induced thermal effects or nonlinear effects in polymers and liquid crystals [9, 36, 37].

4.2 Orientational ordering: the physical picture

The physical picture for soliton-mediated orientational ordering is illustrated in Figs. 4.1(a) and 4.1(b). Naturally, the nanorod suspension is isotropic at room temperature, which implies that the nanorods are randomly oriented. Once the plasmonic soliton is established, the nanorods experience an optical potential and, thus, reorient with respect to the polarization of the soliton beam, and the rotational degree of freedom is highly suppressed. This configuration is triggered by the soliton-mediated optical torque on the nanorods. A rod can be modeled as a prolate spheroid with a long semi-axis a, and two identical short semi-axes b ($a > b$). The prolate rod is polarized by an electromagnetic field, with the frequency-dependent polarizabilities parallel (along long axis) and perpendicular (along short axis) to the polarization

described by [30, 38]

$$\alpha_{\shortparallel,\perp} = 4\pi ab^2\epsilon_m \frac{\epsilon_1 - \epsilon_m}{3\epsilon_m + 3L_{\shortparallel,\perp}(\epsilon_1 - \epsilon_m)}, \tag{4.1}$$

where ϵ_1 and ϵ_m are the frequency-dependent complex dielectric constants of gold and the surrounding medium. The geometrical structure factor along the longitudinal mode direction is

$$\alpha_{\shortparallel,\perp} = 4\pi ab^2\epsilon_m \frac{\epsilon_1 - \epsilon_m}{3\epsilon_m + 3L_{\shortparallel,\perp}(\epsilon_1 - \epsilon_m)}, \tag{4.2}$$

where the eccentricity e is defined as $e^2 = 1 - b^2/a^2$. The geometric factor along the short axis is $L_\perp = (1 - L_\shortparallel)/2$. For simplicity, let us assume that the rod is initially aligned in the transverse plane [Fig. 4.1(d)]. Naturally, the orientations of nanorods in the suspension are random, resulting in an isotropic phase and, thus, the ensemble average of the orientation angle $\langle\beta\rangle = 0$, where β represents the angle of the director (long axis) with respect to the polarization direction of the soliton beam. From Eq. 4.1 and theoretical calculation [13], it can be determined that the polarizability of gold nanorods at 532 nm wavelength is negative along the long axis, but positive along the short axis [Fig. 4.1(c)].

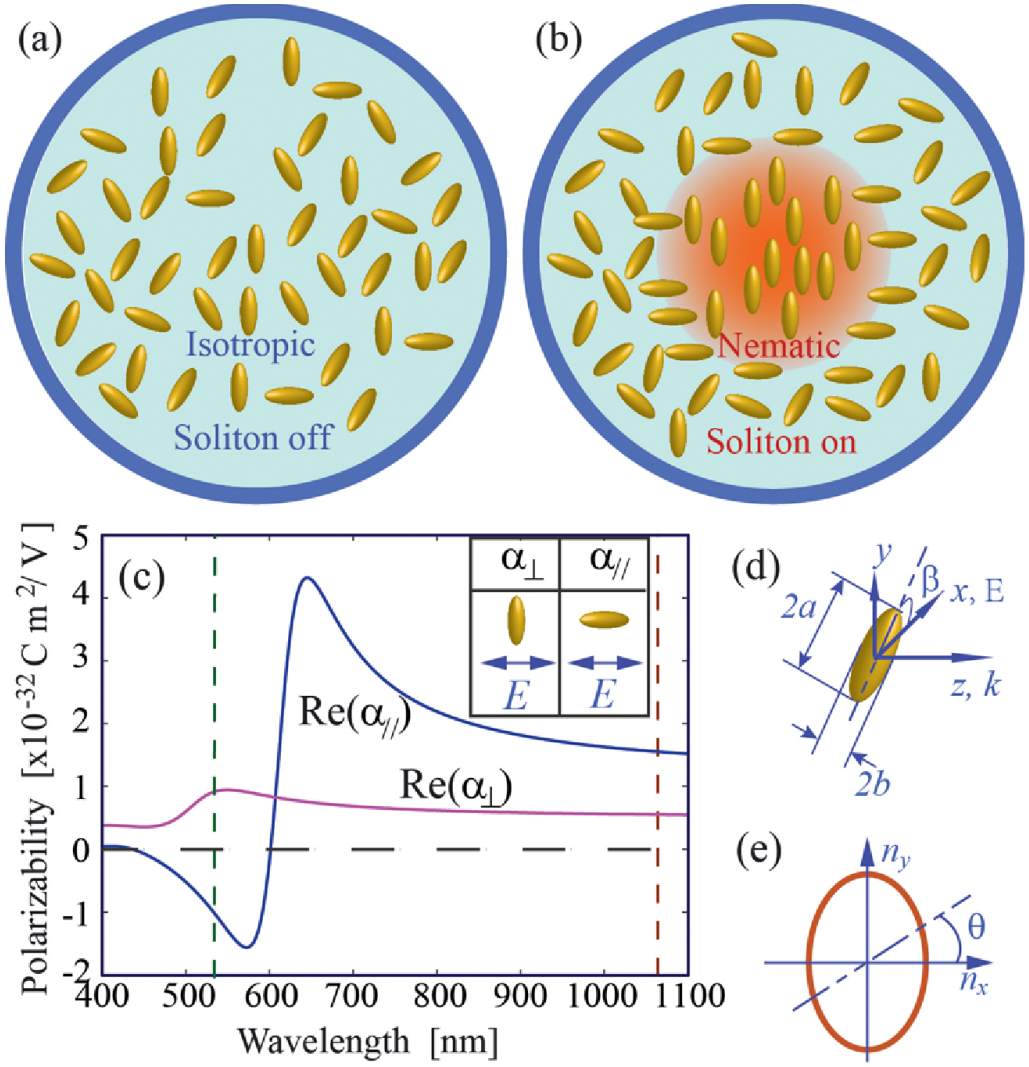

Figure 4.1: Soliton beam rotates nanorods and aligns their long axes toward the direction perpendicular to the laser polarization (nematic phase).

Fig. 4.1. (a) Gold nanorods naturally assume random orientations in the aqueous solution (isotropic phase). (b) Soliton beam rotates nanorods and aligns their long

axes toward the direction perpendicular to the laser polarization (nematic phase) due to optical torque from the soliton beam. (c) Parallel and perpendicular polarizabilities of a single nanorod as a function of the laser wavelength, showing opposite polarizabilities at 532 nm (marked by left dashed line). The right dashed line marks the probe beam wavelength at 1064 nm. (d) Schematic of the rod orientation with β being the angle between the long axis of the nanorod and the polarization of the soliton beam (the x-axis). (e) Illustration of refractive indices in the orthogonal directions due to induced optical anisotropy. The dashed line shows the polarization direction (angle θ) of the incident probe beam.

As we can see in Fig. 4.1, those rods with the long axis aligned in parallel with the beam polarization will be repelled, while those with the long axis perpendicular to the beam polarization will be attracted by the soliton beam [5, 10]. For those rods that are initially oriented in other arbitrary directions, the optical torque will rotate them so their long axes can be aligned to the perpendicular direction.

4.3 Optical torque and transmitted power

In theory, the misalignment between the induced dipole moment of a nanorod $\overrightarrow{P}$ and the optical field $\overrightarrow{E}$ results in a torque $\tau = \overrightarrow{P} \times \overrightarrow{E}$, which is proportional to the polarizability difference $\Delta\alpha = \alpha_{\shortparallel} - \alpha_{\perp}$ in the Rayleigh particle regime [39]. The rotational motion of the nanorod is typically described by the Langevin equation [39], $I\frac{d^2\beta}{dt^2} = N\sin^2\beta - \gamma\frac{d\beta}{dt}$, where I is the nanorod moment of inertia, β is the

orientation angle, as defined before, $N = -\Delta\alpha E^2/4$ is the time-averaged torque amplitude, and γ is the angular drag coefficient from the Stokes law for rotation in a viscous medium. Clearly, in the waveguide channel induced by the soliton beam, the torque exerted by the soliton beam depends on the local intensity (as E^2 is the squared magnitude of the optical field). Results from our calculation of the torque are presented below.

We examine orientational ordering and associated optical birefringence by measuring the transmission of a probe beam with varying linear polarization through the soliton-induced waveguide channel. The optical property of the nanorods within the waveguide can be expressed as a refractive index ellipsoid analog to the birefringent crystal, with n_x and n_y being the two complex refractive indices along the principal axes [Fig. 4.1(e)]. In combination with the Malus law, the output power of the linearly polarized components of the probe beam along the principal axes can be written as

$$P_x = P_{\text{in}}\cos^2(\theta)\exp\left(-\text{Im}\left(n_x\right)L_{\text{opt}}\right), \tag{4.3}$$

$$P_y = P_{\text{in}}\sin^2(\theta)\exp\left(-\text{Im}\left(n_y\right)L_{\text{opt}}\right), \tag{4.4}$$

where $L_{\text{opt}} = 2\pi L/\lambda$ is phase that the light accumulates when passing through the cuvette (length L) without the medium. Im stands for the imaginary part. The total output power is $P_s = P_x + P_y$; thus, the transmission spectrum $T(\theta) = P_s/P_{\text{in}}$

will be simplified as

$$T = \exp\left(-2\mathrm{Im}\left(n_x\right) L_{\mathrm{opt}}\right) + \sin^2\left(\theta\right)\left[\exp\left(-\mathrm{Im}\left(n_y\right) L_{\mathrm{opt}}\right) - \exp\left(-\mathrm{Im}\left(n_x\right) L_{\mathrm{opt}}\right)\right] \tag{4.5}$$

Since the absorption of water is unlikely orientation dependent, in the transmission spectra, the global absorbance of water is neglected as we focus on distinguishing between optically induced nematic and isotropic phases of nanorods. The introduction of the soliton beam apparently enhances the optical transparency as shown in our transmission measurement. More interestingly, the refractive index experienced by the probe beam in the soliton-induced waveguide channel exhibits birefringence, producing polarization-dependent transmission of light according to Eq. 4.5. A modulation depth,

$$\eta = exp\left(-\mathrm{Im}\left(n_y\right) L_{\mathrm{opt}}\right) - exp\left(-\mathrm{Im}\left(n_x\right) L_{\mathrm{opt}}\right), \tag{4.6}$$

can be used to distinguish different phases. If no birefringence exists as in the isotropic phase, there will be no polarization-dependent modulation in the transmission measurement. (Recall that such a modulation vanishes in birefringent crystals for which there is no appreciable imaginary index.) We will next use these ideas to perform experimentats to measure these ordering induced changes.

4.4 Orientational ordering: experimental setup

Our experimental setup is shown in Fig. 4.2(a).

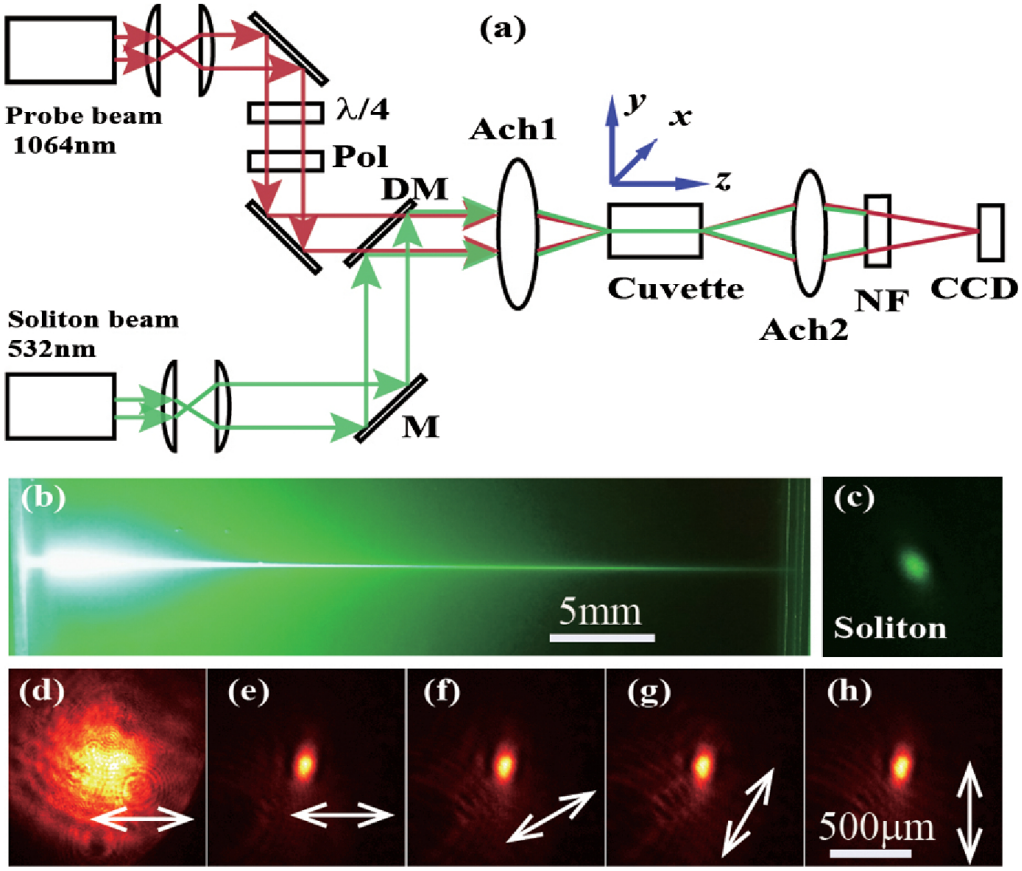

Figure 4.2: (a) Schematic diagram of the experimental setup for soliton mediated phase transition.

Fig. 4.2. (a) Schematic diagram of the experimental setup for soliton mediated phase transition. The soliton-forming beam (532 nm) is collimated to 5 mm in diameter and then focused by an achromatic lens (Ach1) onto the input facet of

the cuvette containing nanosuspension. A probe beam (1064 nm) at low power is sent through a dichroic mirror (DM), propagating collinearly with the green beam, and its polarization is regulated by a quarter-waveplate and a polarizer. The output intensity patterns of the IR beam are taken by a CCD camera, together with another achromatic lens (Ach2) and a notch filter (NF). (b), (c) Side view image of the green soliton beam and its zoom-in self-trapped transverse pattern. (d)–(h) Linear diffraction (d) and guided output of the probe beam (e–h) with its polarization angle θ at 0°, 30°, 60° and 90°.

The gold nanorods used in this experiment have an average diameter of 50 nm and a length of 100 nm, which corresponds to a transverse surface plasmonic resonance (TSPR) at 520 nm, but an LSPR at 600 nm. A linearly polarized green soliton forming beam at wavelength 532 nm (blue-detuned with respect to the LSPR) is focused to around 20 μm (FWHM) at the entrance surface of the suspension in a 40 mm long cuvette by an achromatic lens with an 80 mm focal length. The output spatial transverse patterns are monitored by another achromatic lens ($f = 200mm$), together with a CCD camera. At low input power, the green beam undergoes linear diffraction to a beam size of 1.4 mm, but as the power is increased to only 100 mW, a needle-like soliton channel is formed as seen from the side view image shown in Fig. 4.2(b). The zoom-in output pattern of the soliton beam shows a much reduced beam size [Fig. 4.2(c)]. These soliton results agree with our previous observations [16] but, in what follows, we focus on the orientational ordering effect induced by

optical torques.

4.5 Measuring the polarization transmission spectrum

To measure the polarization transmission spectrum in order to facilitate the detection of the soliton-mediated phase transition described above, an IR probe beam (1064 nm) is launched into the soliton waveguide created by the 532 nm beam [16]. The IR beam is prepared to be circularly polarized, but then passes through a rotary polarizer, which allows the probe beam to have nearly constant power when its polarization direction is varied. The IR probe beam is set at a fairly low power (∼10 mW), so it does not have any nonlinear self-action in the nanorod suspension. Typical guided output patterns of the weak IR beam with different polarization directions are shown in the bottom panels of Fig. 4.2, where Fig. 4.2(d) shows the natural linear diffraction of the probe beam when the soliton beam is absent, and Figs. 4.2(e)–4.2(h) show the guided output patterns when the soliton beam is turned on. The probe beam with different polarization orientations (0°, 30°, 60° and 90°) is always guided in the soliton channel, as it experiences a higher refractive index along the soliton channel. The controlled polarization orientation facilitates the detection of the birefringence due to isotropic to nematic phase transition. This is done simply by measuring the transmitted power with a power meter placed in the output beam path after the green soliton beam is blocked by a notch filter.

Figure 4.3 shows the typical measured polarization transmission spectrum. For

these results, the input power for both the soliton beam and the probe is fixed, and the only variable is the input polarization of the probe beam.

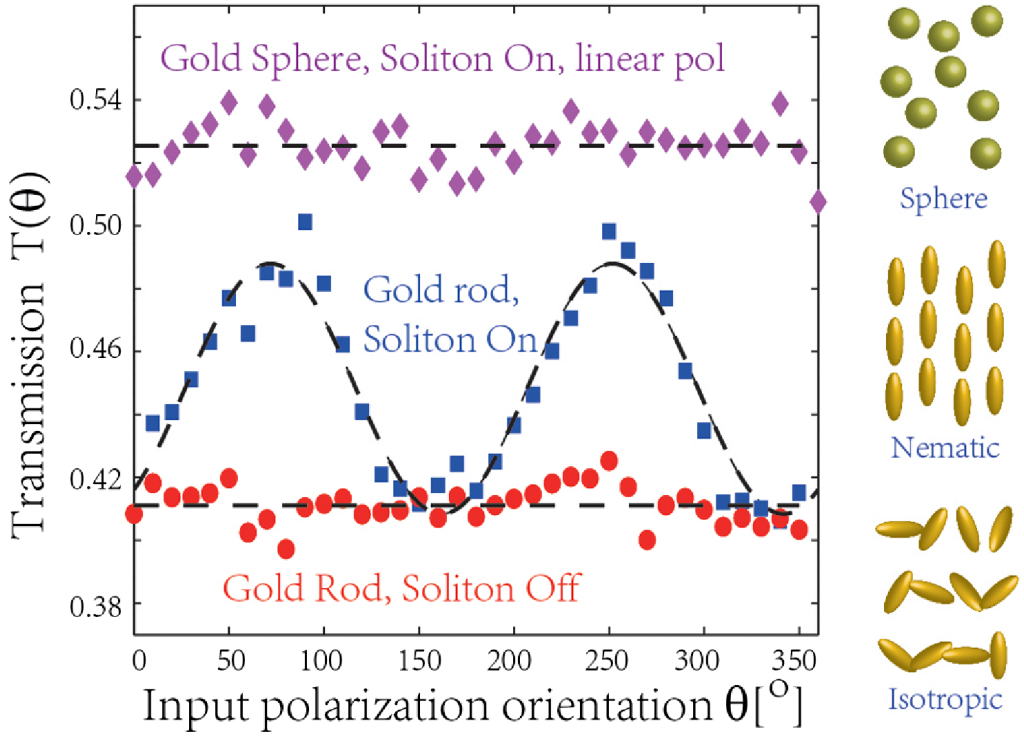

Figure 4.3: Polarization transmission spectrum of the probe beam.

Fig. 4.3.Polarization transmission spectrum of the probe beam measured when the soliton beam is turned on (blue squares) and off (red dots) in a gold nanorod suspension, indicating orientational ordering from isotropic phase to nematic phase by the action of the soliton beam. The spectrum from a gold nanosphere suspension shows no appreciable modulation even with the soliton beam on (magenta diamonds).

The transmission (normalized to input power) is strongly modulated when the soliton beam is on, but remains fairly flat when the soliton beam is off. These results are in agreement with the prediction from Eq. 4.5. If we vary the input power of the soliton beam, the modulation depth becomes appreciable only when strong nonlinear self-trapping is achieved at high power levels around 100 mW, indicating that orientational ordering and resulting birefringence arise from the action of the soliton beam. For direct comparison, we also plot in Fig. 4.3 results obtained from gold nanosphere suspensions. The measured data points are fitted with the same sinusoidal model for both the on and off cases of the soliton beam, and it is found that the amplitude of modulation increased about 10 times from the off-to-on transition for the nanorods but, for nanospheres, the modulation (mainly due to experimental noise) kept in the level, since n_x and n_y are the same for nanospheres.

4.6 Rod alignment

To have a quantitative understanding of the alignment process of nanorods under the action of a laser beam, we perform finite element calculations of the force and torque acting on a single nanorod. Shown in Fig. 4.4(a) is the torque exerted on a nanorod placed at the focus of the laser beam as a function of the orientation angle β, as defined in Fig. 4.1(b).

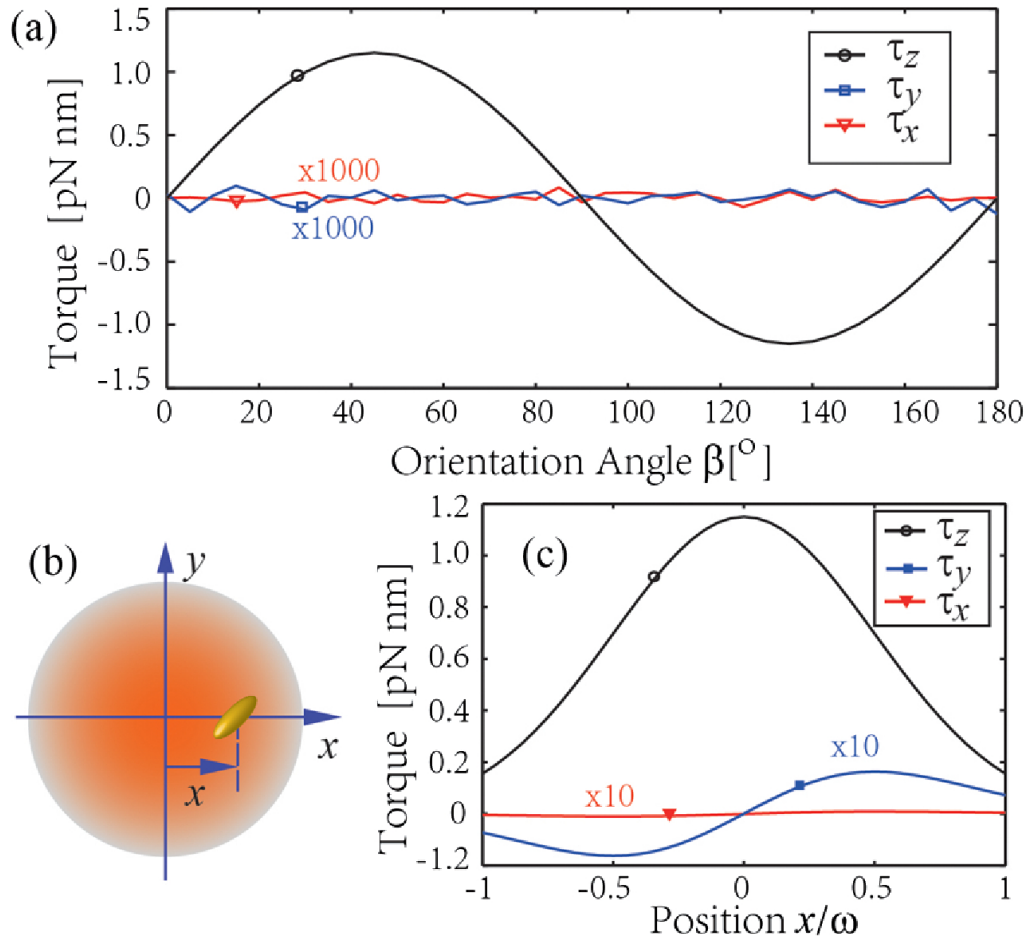

Figure 4.4: Calculated torque exerted by the soliton beam on a single gold nanorod at the beam center with different orientations.

Fig. 4.4. (a) Calculated torque exerted by the soliton beam on a single gold nanorod at the beam center with different orientations. Note that torques in the x and y directions are magnified by a factor of 1000 for easy comparison. (b) Schematic of the position and orientation of a single nanorod located off the beamcenter and

(c) the torque exerted on the nanorod as a function of the displacement x normalized by the beam waist ω from the beam center (the orientation of the rod is fixed). The torques along the x and y directions are magnified by a factor of 10.

The torque along the z-direction is much larger than that in the transverse directions, and changes its direction from counter-clockwise to clockwise when β increases over 90° This clearly indicates that a nanorod tends to align its long axis perpendicular to the soliton beam polarization. Our calculations show that this alignment process still occurs when the nanorod is placed away from the beam focus along the lateral direction [Figs. 4.4(b) and 4.4(c)]. Experimentally, we also estimated the real part of the birefringence by sending a 45° linearly polarized beam into the nanorod suspension and measuring the output power after a polarization analyzer. The measured phase shift between two orthogonal polarization components is about 1° indicating the birefringence in nanorod suspensions is quite small. To see if this alignment process is affected by the polarization of the soliton beam, we perform similar polarization transmission measurement in the soliton-induced waveguide, but with the soliton beam being circularly polarized. Figures 4.5(a) and 4.5(b) show the output transverse intensity patterns of linear diffraction and soliton formation of the circularly polarized green beam.

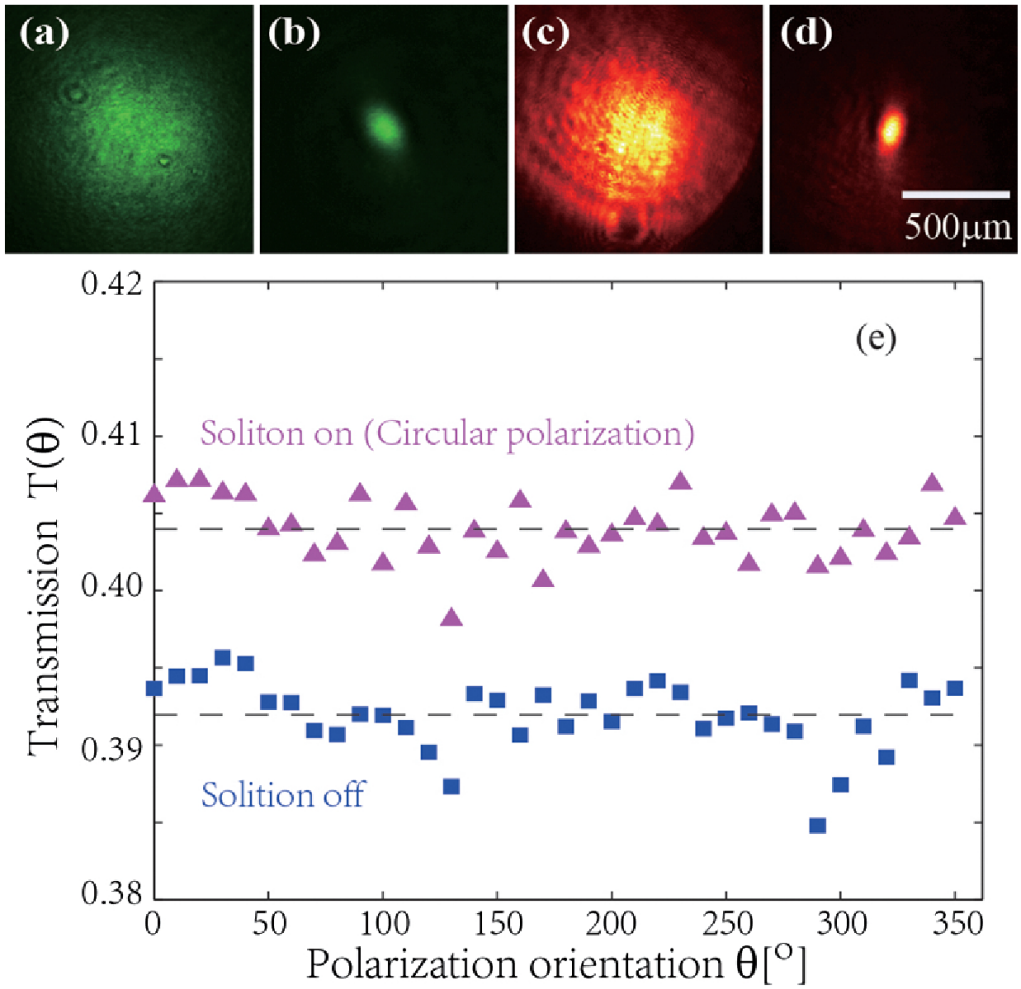

Figure 4.5: Transverse output intensity patterns of a circularly polarized green beam showing linear diffraction at low power and nonlinear self-trapping at high power.

Fig. 4.5. Transverse output intensity patterns of a circularly polarized green beam showing (a) linear diffraction at low power and (b) nonlinear self-trapping at high power. (c), (d) Corresponding output patterns of the IR probe beam when

the soliton beam is off and on, respectively. (e) Polarization transmission spectra show no significant difference when the soliton beam is turned on or off provided it is circularly polarized.

As shown in Figs. 4.5(c) and 4.5(d), the IR probe beam is also guided by the soliton-induced waveguide channel. The measured polarization spectrum is shown in Fig. 4.5(e), which displays no appreciable difference between the cases when the soliton beam is on and off. This suggests that the circularly polarized soliton beam does not induce orientational ordering of the nanorods as expected.

Chapter 5

Conclusion

In conclusion, we have observed the guiding of an IR light beam in a self-trapped green beam in a plasmonic nanosuspension composed of either gold spheres or rods. We have also demonstrated nonlinear coupling of two beams in gold nanoshell suspensions. The fact that a weak visible beam can guide an intense invisible beam in a variety of colloidal suspensions could be of interest and may bring about new possibilities for applications in optical manipulation, as well as optofluidics and biophotonics. We have also demonstrated soliton-mediated orientational ordering and birefringence in nonlinear gold nanorod suspensions. The orientation of the nanorods is disordered in a natural suspension, as driven by Brownian motion. Within the soliton induced waveguide channel, however, the rotational fluctuation of the rods is suppressed, and the rods are aligned due to the optical torque resulting from the soliton beam. The concept of soliton mediated ordering may be applied in other nonlinear colloidal and optofluidic systems, and may find applications in manipulation

of light-matter interaction through plasmonic coupling.

Chapter 6

Publications

1. Yu-Xuan Ren, Trevor S. Kelly, Chensong Zhang, Huizong Xu, Zhigang Chen. Soliton-mediated orientational ordering of gold nanorods and birefringence in plasmonic suspensions, Optics letters Vol. 42, Issue 3, pp. 627-630, February 2017.

2. Trevor S. Kelly, Yu-Xuan Ren, Akbar Samadi, Anna Bezryadina, Demetrios Christodoulides, Zhigang Chen. Guiding and nonlinear coupling of light in plasmonic nanosuspensions, Optics letters Vol. 41, Issue 16, pp. 3817-3820, August 2016.

Chapter 7

Conference presentations

1. Y. Ren, T. Kelly (Presenter), Chensong Zhang, Huizong Xu, Zhigang Chen. "Soliton-mediated orientational ordering of gold nanorods and birefringence in plasmonic suspensions," in Conference on Lasers and Electro-Optics (CLEO), (Optical Society of America, 2017).

2. Y. Ren, Josh Lamstein (Presenter), T. Kelly, Chensong Zhang, Yong Sun, Claudio Conti, Demetrios N. Christodoulides, and Zhigang Chen. "Rogue waves in red blood cell suspensions," in Conference on Lasers and Electro-Optics (CLEO), (Optical Society of America, 2017).

3. Y. Ren, T. Kelly (Presenter), A. Samadi, A. Bezryadina, D. N. Christodoulides, and Z. Chen. "Guiding and Coupling Light through Nonlinear Plasmonic Nanosuspensions," in Conference on Lasers and Electro-Optics (CLEO), (Optical Society of

America, 2016).

4. Trevor S. Kelly, (Presenter), Akbar Samadi, Anna Bezryadina and Zhigang Chen. Guiding light by plasmonic resonant solitons in metallic nanosuspensions, SPIE 9546, Active Photonic Materials VII, 95461R (September 1 2015).

Bibliography

[1] A. Ashkin, J. M. Dziedzic, and P. W. Smith. Continuous-wave self-focusing and self-trapping of light in artificial kerr media. *Opt. Lett.*, 7(6):276–278, Jun 1982.

[2] Zhigang Chen, Mordechai Segev, and Demetrios N Christodoulides. Optical spatial solitons: historical overview and recent advances. *Reports on Progress in Physics*, 75(8):086401, 2012.

[3] Claudio Conti, Giancarlo Ruocco, and Stefano Trillo. Optical spatial solitons in soft matter. *Phys. Rev. Lett.*, 95:183902, Oct 2005.

[4] P. J. Reece, E. M. Wright, and K. Dholakia. Experimental observation of modulation instability and optical spatial soliton arrays in soft condensed matter. *Phys. Rev. Lett.*, 98:203902, May 2007.

[5] R. El-Ganainy, D. N. Christodoulides, C. Rotschild, and M. Segev. Soliton dynamics and self-induced transparency in nonlinear nanosuspensions. *Opt. Express*, 15(16):10207–10218, Aug 2007.

[6] Michał Matuszewski, Wieslaw Krolikowski, and Yuri S. Kivshar. Spatial solitons and light-induced instabilities in colloidal media. *Opt. Express*, 16(2):1371–1376, Jan 2008.

[7] W. M. Lee, R. El-Ganainy, D. N. Christodoulides, K. Dholakia, and E. M. Wright. Nonlinear optical response of colloidal suspensions. *Opt. Express*, 17(12):10277–10289, Jun 2009.

[8] R. El-Ganainy, D. N. Christodoulides, E. M. Wright, W. M. Lee, and K. Dholakia. Nonlinear optical dynamics in nonideal gases of interacting colloidal nanoparticles. *Phys. Rev. A*, 80:053805, Nov 2009.

[9] C. Conti and E. DelRe. Optical supercavitation in soft matter. *Phys. Rev. Lett.*, 105:118301, Sep 2010.

[10] Weining Man, Shima Fardad, Ze Zhang, Jai Prakash, Michael Lau, Peng Zhang, Matthias Heinrich, Demetrios N. Christodoulides, and Zhigang Chen. Optical nonlinearities and enhanced light transmission in soft-matter systems with tunable polarizabilities. *Phys. Rev. Lett.*, 111:218302, Nov 2013.

[11] Shima Fardad, Matthew S. Mills, Peng Zhang, Weining Man, Zhigang Chen, and D. N. Christodoulides. Interactions between self-channeled optical beams in soft-matter systems with artificial nonlinearities. *Opt. Lett.*, 38(18):3585–3587, Sep 2013.

[12] Elad Greenfield, Jonathan Nemirovsky, Ramy El-Ganainy, Demetri N. Christodoulides, and Mordechai Segev. Shockwave based nonlinear optical manipulation in densely scattering opaque suspensions. *Opt. Express*, 21(20):23785–23802, Oct 2013.

[13] Shima Fardad, Alessandro Salandrino, Matthias Heinrich, Peng Zhang, Zhigang Chen, and Demetrios N. Christodoulides. Plasmonic resonant solitons in metallic nanosuspensions. *Nano Letters*, 14(5):2498–2504, 2014. PMID: 24697412.

[14] Roland A. Terborg, Juan P. Torres, and Karen Volke-Sepulveda. Steering and guiding light with light in a nanosuspension. *Opt. Lett.*, 38(24):5284–5287, Dec 2013.

[15] Albert S. Reyna and Cid B. de Araújo. Guiding and confinement of light induced by optical vortex solitons in a cubic quintic medium. *Opt. Lett.*, 41(1):191–194, Jan 2016.

[16] Trevor S. Kelly, Yu-Xuan Ren, Akbar Samadi, Anna Bezryadina, Demetrios Christodoulides, and Zhigang Chen. Guiding and nonlinear coupling of light in plasmonic nanosuspensions. *Opt. Lett.*, 41(16):3817–3820, Aug 2016.

[17] Ming feng Shih, Zhigang Chen, Matthew Mitchell, Mordechai Segev, Howard Lee, Robert S. Feigelson, and Jeffrey P. Wilde. Waveguides induced by photorefractive screening solitons. *J. Opt. Soc. Am. B*, 14(11):3091–3101, Nov 1997.

[18] Marcus Asaro, Michael Sheldon, Zhigang Chen, Oksana Ostroverkhova, and W. E. Moerner. Soliton-induced waveguides in an organic photorefractive glass. *Opt. Lett.*, 30(5):519–521, Mar 2005.

[19] Zhigang Chen, Tamer H. Coskun, Demetrios N. Christodoulides, and Mordechai Segev. Observation of incoherently coupled photorefractive spatial soliton pairs. *Opt. Lett.*, 21(18):1436–1438, Sep 1996.

[20] Yu-Xuan Ren, Trevor S. Kelly, Chensong Zhang, Huizhong Xu, and Zhigang Chen. Soliton-mediated orientational ordering of gold nanorods and birefringence in plasmonic suspensions. *Opt. Lett.*, 42(3):627–630, Feb 2017.

[21] Alexandr Jon and Pavel Zemnek. Light at work: The use of optical forces for particle manipulation, sorting, and analysis. *ELECTROPHORESIS*, 29(24):4813–4851, 2008.

[22] Xiaohua Huang, Ivan H. El-Sayed, Wei Qian, and Mostafa A. El-Sayed. Cancer cell imaging and photothermal therapy in the near-infrared region by using gold nanorods. *Journal of the American Chemical Society*, 128(6):2115–2120, 2006. PMID: 16464114.

[23] Wei-Shun Chang, Ji Won Ha, Liane S. Slaughter, and Stephan Link. Plasmonic nanorod absorbers as orientation sensors. *Proceedings of the National Academy of Sciences*, 107(7):2781–2786, 2010.

[24] M. E. J. Friese, T. A. Nieminen, N. R. Heckenberg, and H. Rubinsztein-Dunlop. Optical alignment and spinning of laser-trapped microscopic particles. *Nature*, 394(6691):348–350, July 1998.

[25] Arthur La Porta and Michelle D. Wang. Optical torque wrench: Angular trapping, rotation, and torque detection of quartz microparticles. *Phys. Rev. Lett.*, 92:190801, May 2004.

[26] Anni Lehmuskero, Peter Johansson, Halina Rubinsztein-Dunlop, Lianming Tong, and Mikael Kll. Laser trapping of colloidal metal nanoparticles. *ACS Nano*, 9(4):3453–3469, 2015. PMID: 25808609.

[27] Yoshito Tanaka, Hiroyuki Yoshikawa, Tamitake Itoh, and Mitsuru Ishikawa. Laser-induced self-assembly of silver nanoparticles via plasmonic interactions. *Opt. Express*, 17(21):18760–18767, Oct 2009.

[28] Matthew Pelton, Mingzhao Liu, Hee Y. Kim, Glenna Smith, Philippe Guyot-Sionnest, and Norbert F. Scherer. Optical trapping and alignment of single gold nanorods by using plasmon resonances. *Opt. Lett.*, 31(13):2075–2077, Jul 2006.

[29] Christine Selhuber-Unkel, Inga Zins, Olaf Schubert, Carsten Snnichsen, and Lene B. Oddershede. Quantitative optical trapping of single gold nanorods. *Nano Letters*, 8(9):2998–3003, 2008. PMID: 18720978.

[30] P. V. Ruijgrok, N. R. Verhart, P. Zijlstra, A. L. Tchebotareva, and M. Orrit. Brownian fluctuations and heating of an optically aligned gold nanorod. *Phys. Rev. Lett.*, 107:037401, Jul 2011.

[31] Jiunn-Woei Liaw, Ying-Syuan Chen, and Mao-Kuen Kuo. Maxwell stress induced optical torque upon gold prolate nanospheroid. *Applied Physics A*, 122(3):182, Feb 2016.

[32] Jaekwon Do, Michael Fedoruk, Frank Jckel, and Jochen Feldmann. Two-color laser printing of individual gold nanorods. *Nano Letters*, 13(9):4164–4168, 2013. PMID: 23927535.

[33] Jan Trojek, Lukáš Chvátal, and Pavel Zemánek. Optical alignment and confinement of an ellipsoidal nanorod in optical tweezers: a theoretical study. *J. Opt. Soc. Am. A*, 29(7):1224–1236, Jul 2012.

[34] Ke Wang, Seon-Mi Jin, Jiangping Xu, Ruijing Liang, Khurram Shezad, Zhigang Xue, Xiaolin Xie, Eunji Lee, and Jintao Zhu. Electric-field-assisted assembly of polymer-tethered gold nanorods in cylindrical nanopores. *ACS Nano*, 10(5):4954–4960, 2016. PMID: 27054687.

[35] Qingkun Liu, Yanxia Cui, Dennis Gardner, Xin Li, Sailing He, and Ivan I. Smalyukh. Self-alignment of plasmonic gold nanorods in reconfigurable anisotropic fluids for tunable bulk metamaterial applications. *Nano Letters*, 10(4):1347–1353, 2010. PMID: 20334353.

[36] Yuval Lamhot, Assaf Barak, Or Peleg, and Mordechai Segev. Self-trapping of optical beams through thermophoresis. *Phys. Rev. Lett.*, 105:163906, Oct 2010.

[37] A. Piccardi, U. Bortolozzo, S. Residori, and G. Assanto. Spatial solitons in liquid-crystal light valves. *Opt. Lett.*, 34(6):737–739, Mar 2009.

[38] Craig F. Bohren and Donald R. Huffman. *Particles Small Compared with the Wavelength*, pages 130–157. Wiley-VCH Verlag GmbH, 2007.

[39] W. Andrew Shelton, Keith D. Bonin, and Thad G. Walker. Nonlinear motion of optically torqued nanorods. *Phys. Rev. E*, 71:036204, Mar 2005.